frontiers | Frontiers in Materials

TYPE Original Research
PUBLISHED 15 September 2022
DOI 10.3389/fmats.2022.965772

OPEN ACCESS

EDITED BY
M. K. Samal,
Bhabha Atomic Research Centre (BARC), India

REVIEWED BY
Citlalli Gaona-Tiburcio,
Autonomous University of Nuevo León, Mexico
Ping Duan,
China University of Geosciences Wuhan, China
Sagar Chandra,
Homi Bhabha National Institute, India

*CORRESPONDENCE
Pan Wang,
wangpan@qut.edu.cn

SPECIALTY SECTION
This article was submitted to Computational Materials Science, a section of the journal Frontiers in Materials

RECEIVED 10 June 2022
ACCEPTED 31 August 2022
PUBLISHED 15 September 2022

CITATION
Hu X, Zheng H, Tao R and Wang P (2022), Migration of nitrite corrosion inhibitor in calcium silicate hydrate nanopore: A molecular dynamics simulation study.
Front. Mater. 9:965772.
doi: 10.3389/fmats.2022.965772

Migration of nitrite corrosion inhibitor in calcium silicate hydrate nanopore: A molecular dynamics simulation study

Xiaoxia Hu, Heping Zheng, Rui Tao and Pan Wang*

Department of Civil Engineering, Qingdao University of Technology, Qingdao, China

Nitrite is an effective corrosion inhibitor that can inhibit the corrosion of steel reinforcement and extend the service life of reinforced concrete. The transport speed of nitrite in the cement micro-porous channels determines the anti-corrosion effect of reinforcing steel. In this paper, the transport behavior of three nitrite corrosion inhibitors, namely $LiNO_2$, $Ca(NO_2)_2$, and $NaNO_2$, in cement micro-porous channels is investigated based on molecular dynamics simulations and finds that NO_2^- in $LiNO_2$ has the fastest transport speed in the channels. The ions' local structure and dynamic behavior of ions analysis reveal that ion clusters and pores adsorption determine the speed of ion transport. Compared with the other two nitrites, the Li ions have the weakest ability to capture NO_2^- and form the most unstable clusters (NO_2^--Li-water) in the $LiNO_2$ solution. Meanwhile, the coordination numbers results indicate that water in $LiNO_2$ provides the most potent driving force. These phenomena reasonably explain the fastest transport speed of NO_2^- through the pores in $LiNO_2$ solution. The transport behavior of corrosion inhibitors in the micro-porous channels is thoroughly decoded at the atomic level, which is instrumental in solving the problem of the optimal corrosion inhibitor selecting for the design of highly durable concrete.

KEYWORDS

molecular dynamics simulation, nitrite corrosion inhibitor, hydrated calcium silicate, transport behavior, CSH (calcium silicate hydrate)

1 Introduction

The concrete environment has high alkalinity, with a pH between 12 and 13, producing a layer of a self-protecting passivation film on the internal steel reinforcement surface (Page and Treadaway, 1982). As one of the main products of cement hydration, Calcium hydroxide ($Ca(OH)_2$) can prevent the passivation film of steel from being destroyed (Page, 1975). However, as the concrete carbonizes or the pH value of the internal environment decreases significantly, the passivation film is destroyed, and the corrosion cell is formed on the surface of the steel (Bažant, 1979).

The overview of the entire corrosion process reveals that the Cl^- is not consumed in the corrosion process but acts as a catalyst to promote corrosion (Thangavel and

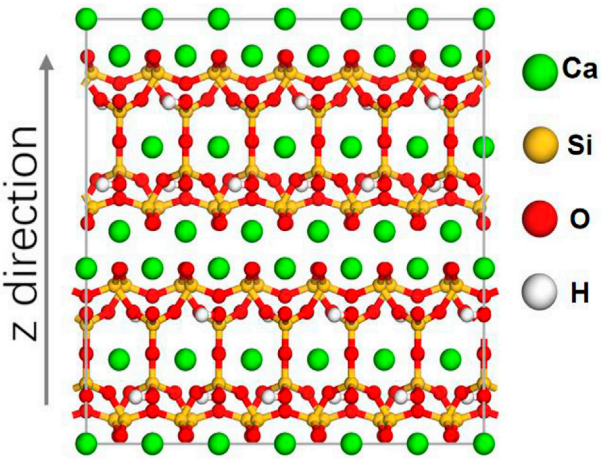

FIGURE 1
The tobermorite 11 Å origin cell. The green, yellow red, white spheres represent the calcium, silicon and hydrogen, respectively.

Rengaswamy, 1998). As a result, even a small amount of Cl^- existing can trigger pitting corrosion. Care et al. (2008) found that the volume of steel reinforcement expanded by 6.5 times after corrosion, which causes cracking and peeling of the concrete, thus significantly reducing the load-bearing capacity and durability of the component.

Corrosion inhibitors, which can effectively prevent the corrosion of steel bars, are widely used in the concrete industry (Ormellese et al., 2011; Aydin and Cizmeciglu, 2015; Diamanti et al., 2017; Sun et al., 2019). The widely used corrosion inhibitors include phosphate (Mandal et al., 2020), chromate (Schiessl et al., 2008; Okeniyi et al., 2014), zinc oxide (Devi and Kannan, 2013), gluconate (Li et al., 2015), amines (Qian and Cusson, 2004), nitrite (Krolikowski and Kuziak, 2011; Mandal et al., 2020), and so on (Soylev and Richardson, 2008). Gonzalez compared the different corrosion inhibitors and found that nitrite corrosion inhibitors have a more significant corrosion inhibiting effect than the others (González et al., 1998). So, a lot of research has been carried out on different kinds of nitrite corrosion inhibitors (Garces et al., 2008; Krolikowski and Kuziak, 2011). Ryu found that adding $Ca(NO_2)_2$ into reinforced concrete can improve the corrosion resistance, shorten the final setting time and improve the early strength (Ryu et al., 2017a). Garcés investigated the effect of pH and the addition amount of $NaNO_2$ on the corrosion inhibitor effect and found that the corrosion inhibition effect of $NaNO_2$ is reduced by about 10% under alkaline conditions (Garces et al., 2011). Ryu put the steel bar into the mixed solution of $LiNO_2$, $Ca(OH)_2$ and NaCl and found that $LiNO_2$ could perform a significant corrosion inhibition function at different concentrations of saline solution (Ryu et al., 2017b). Ann found that the addition of a nitrite corrosion inhibitor increased the threshold for chloride ions causing corrosion from 0.18%–0.33% to 0.22%–1.95% (Reou and Ann, 2008). Studies show that $LiNO_2$ mixed with concrete can improve the strength and durability of concrete (Hori et al., 1991). Hazehara et al. (2020) found that $LiNO_2$ can improve the working performance of concrete compared with $Ca(NO_2)_2$ corrosion inhibitor. Moreover, $LiNO_2$ can effectively stabilize the internal PH value of concrete. Although the effects of corrosion inhibitors on concrete can be understood through experiments, the transport characteristics of ions of inhibitors in the nano-channels inside concrete from a molecular perspective are still unknown.

Because of the limitations of experimental methods, the molecular dynamics simulations method is used to study the transport behavior of nitrite in nano-channels. MD simulation has been successfully applied to study ion transport behavior in concrete nano-channels channels. Such as, Hou used the method of molecular dynamics simulation to study the transport behavior of chloride ions in concrete microscopic channels. The study found that chloride ions and calcium ions in the channels would form Ca-Cl ion clusters, thus reducing the transport rate of chloride ions. (Hou and Li, 2014). Similarly,

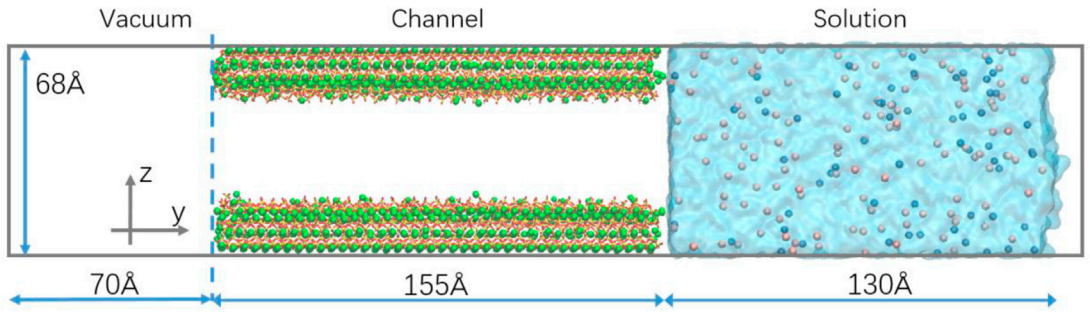

FIGURE 2
The transport model. (The light blue membrane represents the water molecule. The pink and blue balls represent the cation and the NO_2^-, respectively).

10.3389/fmats.2022.965772

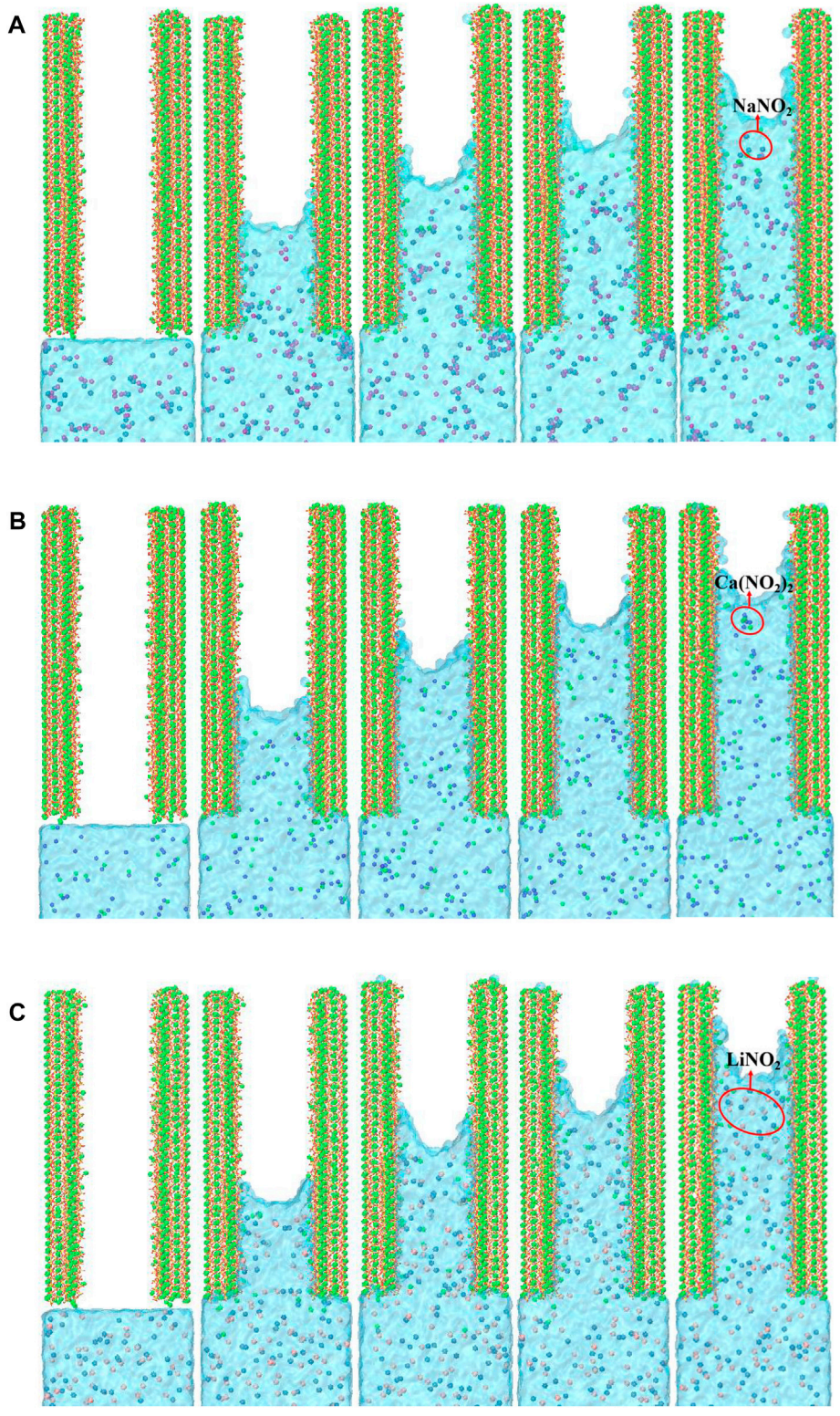

FIGURE 3
Snapshots of the water and ions transport process at 0 ps, 500 ps, 1,000 ps, 1,500 ps, and 2000 ps for **(A)** $NaNO_2$ solution, **(B)** $Ca(NO_2)_2$ solution, and **(C)** $LiNO_2$ solution. (Purple, green, pink and blue balls represent sodium ion, calcium ion, lithium ion and nitrate ion respectively. Besides, The green balls in **(A)** and **(B)** channel solutions are Ca ions dissolved from the CSH substrate).

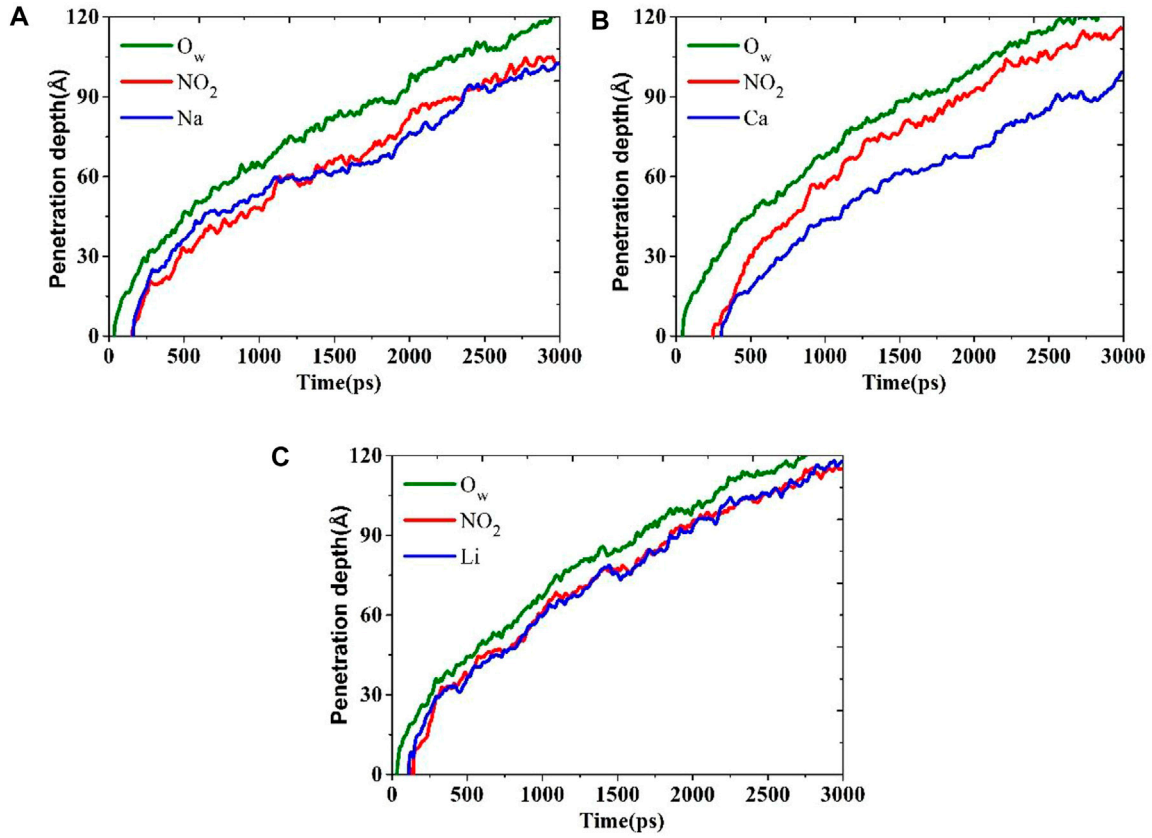

FIGURE 4
Depth of penetration versus time relationship curves: **(A)** $NaNO_2$ solution, **(B)** $Ca(NO_2)_2$ solution and **(C)** $LiNO_2$ solution.

the transport and adsorption properties of Na ions in silicate and aluminosilicate nano-channels are investigated. Na ions can be adsorbed on silicate chains by ionic bonds and form ion clusters with water molecules to block the transport of solution (Hou et al., 2018a). The transport characteristics and principles of salt solution in nano-channels with different pore sizes are also revealed (Yang et al., 2019). The penetration of solutions through different mineral and gel channels is being investigated (Hou et al., 2018b). Yu investigated the effect of graphene oxide epoxy (GO-EP) coating on the transport performance of sodium chloride solution in the micro-porous channels and found that the coating could slow down the transport rate in the pores by forming chemical bonds with Na^+ and Cl^- (Yu et al., 2019). In addition, the microscopic mechanisms of the mechanical properties of polymer-reinforced cementitious materials (Chen et al., 2020) and the interfacial bonding between cementitious and reinforced materials (Wang et al., 2020a; Wang et al., 2020b; Wang et al., 2020c) have also been thoroughly studied based on the MD simulation.

Nitrite will pass through the pores of the concrete itself to reach the surface of the reinforcement, forming a dense film of oxides on the surface of the reinforcement to act as a passivation, thereby improving the durability of the reinforced concrete structure. At present, the effects of different types of nitrite on the properties of reinforced concrete have been tested and verified, and there are very few microscopic studies and mechanism studies on the transport characteristics of nitrite, mainly because it is difficult to study with the help of experimental means at the microscopic scale, and molecular dynamics research can make up for this deficiency. The study of micro-view can more thoroughly elucidate the transport mechanism of nitrite in the internal pores of concrete, thus providing guidance for macroscopic research.

Herein, the transport behavior of lithium nitrite, sodium nitrite, and calcium nitrite in the pores of calcium silicate gels are investigated based on MD simulation. The local structure and dynamic behavior of ions in hydrated calcium silicate (CSH) channels are analyzed to reveal the causes that drive and hinder ion transport and explain the different transport behavior of various nitrite solutions. Expectantly,

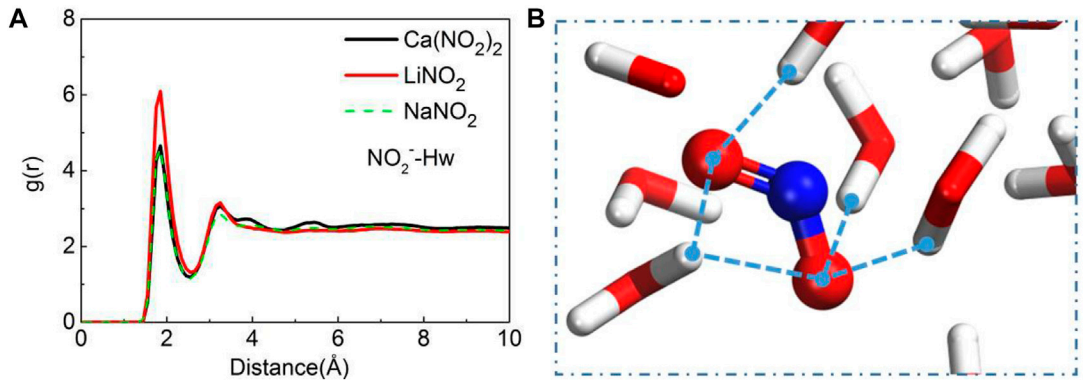

FIGURE 5
The radial distribution function (RDF) of **(A)** NO_2^--H_w and **(B)** the H-bonds network of NO_2^--H_w. (The blue balls are for the nitrogen. The red-white sticks are for the water molecule).

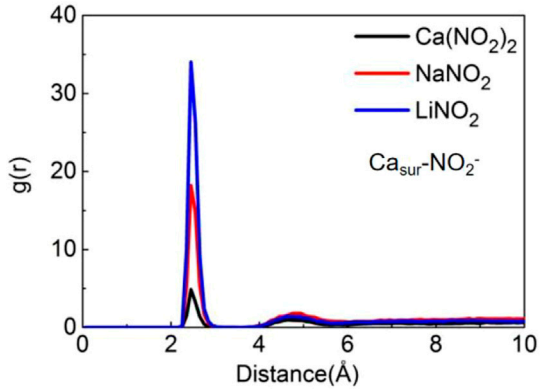

FIGURE 6
The RDFs of Ca_{sur}-NO_2^-.

this work can provide fundamental theoretical support for a comprehensive understanding of the transport behavior of other nitrites corrosion inhibitors in the CSH channels and assist in selecting the optimal corrosion inhibitor for the design of highly durable concrete.

2 Simulation methods

2.1 Model construction

In order to investigate the effects of different cations on the transport behavior of nitrite in CSH gel channel, and to reveal their microscopic mechanisms, three kinds of nitrites, $NaNO_2$, $Ca(NO_2)_2$, and $LiNO_2$ are studied. The transport atom model consists of a vacuum layer, CSH channel and a nitrite solution. Since tobermorite 11 Å has a similar multi-layered structure and the same chemical composition to calcium silicate hydrate (Nonat et al., 1998; Nonat, 2004), it has been used as a substitute for calcium silicate hydrate to study the transport behavior of salt solutions (Zhang et al., 2017). Figure 1 shows the initial model of tobermorite 11 Å with the three-dimensional dimensions of 22.32 Å × 22.17 Å×22.77 Å.

Tobermorite is expanded 7 and 2 times along the *Y and Z* directions, respectively. And then, a calcium silica layer is removed along the Y direction, and the substrates on both sides are shifted outward to form a channel of width 3 nm. Some of the calcium on the surface of the channel is removed, and some of the non-bridged oxygen on the surface is protonated to ensure the charge balance of the channel. A vacuum layer about 7 nm above the CSH substrate is constructed to avoid the influence of periodic boundaries. Three types of nitrite solutions with three-dimensional dimensions of 22.3 Å × 130 Å × 68 Å and a concentration of 1 mol/L are added under CSH substrate, respectively. The final transport model is shown in Figure 2.

2.2 Simulation detail

The hydrated calcium silicate channel is described by the ClayFF force field (Cygan et al., 2004). This force field can accurately describe the interaction of water and salt solutions with cementitious materials or mineral surfaces (Li et al., 2017; Hou et al., 2018b). The Consistent Valence Force Field (CVFF) is utilized to simulation the NO^{2-}, and the geometric rule is selected to unite ClayFF and CVFF force field. This combination to simulate organic additives reinforced cement composites has also been proven to be accurate and feasible (Dauber-Osguthorpe et al., 1988).

Lammps, a large-scale atomic-molecular simulator, is mainly used for molecular dynamics calculation and simulation work. The entire simulation is divided into two stages based on Lammps software: the pre-equilibrium and transport stages

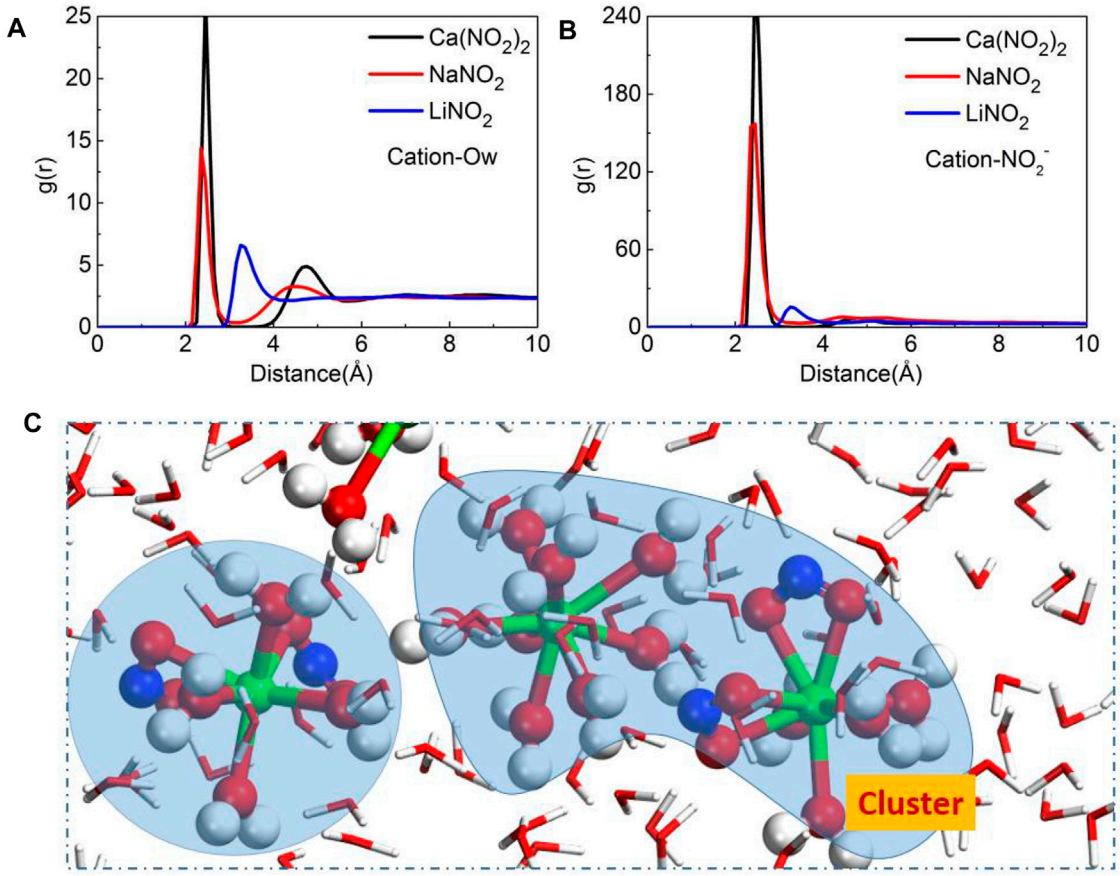

FIGURE 7
The radial distribution function (RDF) of **(A)** Cation-O_w, **(B)** Cation-NO_2^-, **(C)** the ion clusters of the $Ca(NO_2)_2$ solution.

(Plimpton et al., 2007). During the pre-equilibrium stages, the temperature and the time step are set as 300 K and 1 fs, the nitrite solution and the channel are run under the NVT ensemble for 0.5 ns. In order to prevent the solution from entering the CSH channel in the pre-equilibrium stage, a layer of water molecules at the entrance of the CSH channel is fixed. When the whole system reaches equilibrium, the fixed water molecules are completely relaxing, and the nitrite solution is gradually transported into the pore channel by capillary force. The ensemble and the time step remain unchanged during the first stage. The whole transport stage lasts for 3 ns and is saved every 1 ps for data analysis.

3 Results and discussion

3.1 Water and ions transport in the CSH nanopores

The transport process in the CSH nanopore for three kinds of nitrite solutions is presented in Figure 3. Water molecules and ions gradually transport through the CSH gel poles from 0 ps to 2000 ps. During the transport process, the Frontier of the solution exhibits a concave shape. This phenomenon accords with the characteristics of capillary absorption and proves the hydrophilicity of CSH gel. By comparing the screenshots of three solution systems, it can be seen that $LiNO_2$ solution has a slightly more considerable adsorption speed than that of $Ca(NO_2)_2$ solution and $NaNO_2$ solution. Therefore, $LiNO_2$ as a nitrite inhibitor for concrete is widely used due to its rapid transmission speed in the concrete gel nanopore, and it can quickly reach the surface of the steel bar and play an excellent anti-rust role.

In order to quantitatively study the transport process of these nitrite solutions, the movement tracks of the concave surface are monitored, as shown in Figure 4. The depth of penetration versus time relationship curves of water and ions in the CSH nanopores shows a parabolic relation with time, which in line with the traditional capillary adsorption theory of the Lucas-Washburn equation (Ababneh et al., 2013). In the beginning, the ionic penetration curves show a zero-point platform, as shown in Figures 4A,B,C, indicating that no ions are penetrating the gel pore. In addition, there is an overlap of the penetration curves of

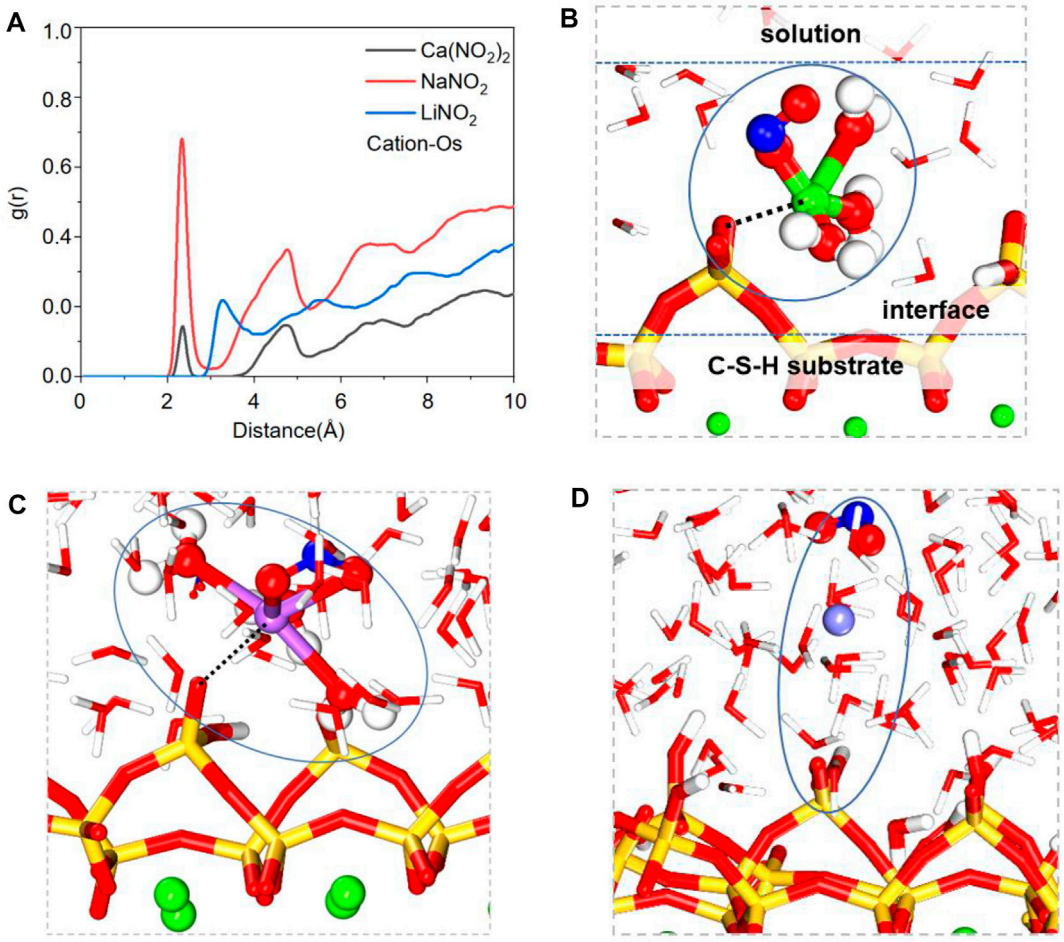

FIGURE 8
(A) The RDF of Cation-O_s, the schematic diagram of **(B)** Ca-O_s, **(C)** Na-O_s and **(D)** Li-O_s.

NO_2^- and cation ions, meaning that the transport of the anions and cations is almost synchronous. There are some similarities between water molecules and ions in transportation, but the migration Frontier of ions always lags behind water molecules, which indicates that ions are dragged upward for transport by water molecules. Meanwhile, the zero-point platform of the $LiNO_2$ is shorter than the other two, and the penetration depth of the NO_2^- in $LiNO_2$ is about 115 Å at 3000 ps, which is similar to $Ca(NO_2)_2$ but more quickly than $NaNO_2$. They demonstrate that the NO_2^- in $LiNO_2$ can enter into nanopore more quickly and has a faster transmission speed.

3.2 Local structure of water and ions

In the first part, the differences in the transport process of three different nitrite solutions in CSH pores are described. Then, the mechanism of the differences in transport behavior will be revealed by analyzing atomic microstructure, chemical bond types, and coordination numbers. The coordination numbers are listed in Table 1.

The local structure of atoms in the system can be characterized by radial distribution function (RDF). During the process of solution permeation, it is found that water molecules drive NO_2^- ions transport forward. In order to compare the differences of water driving force in different nitrite solutions, the RDF of NO_2^--Hw (hydrogen in water) is calculated as shown in Figure 5A. The peaks of NO_2^--Hw in three kinds of nitrite solutions are all located at 1.85 Å, indicating that the H-bonds are developed between them shown in Figure 5B. In $LiNO_2$ solutions, not only the peak of NO_2^--Hw is the highest, but also the coordination number of NO_2^- ions is the largest, which indicates that the interaction between NO_2^- ion and water molecules is the strongest in $LiNO_2$ solution, thereby $LiNO_2$ solution transports the fastest among the three kinds of nitrite solution. In addition, the NO_2^--Hw coordination number in

10.3389/fmats.2022.965772

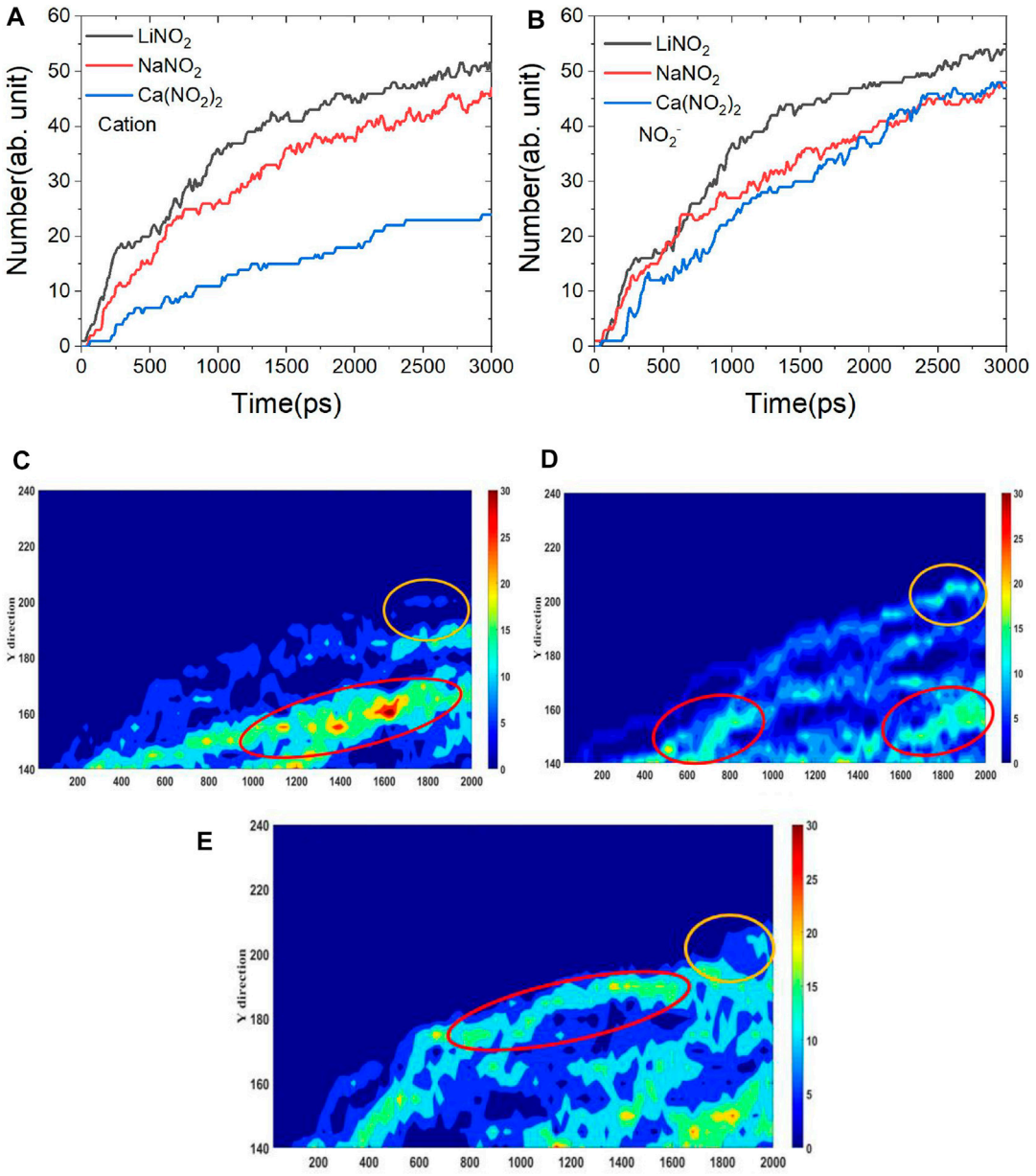

FIGURE 9
The schematic diagram of the number of ions entering the CSH channel over time **(A)** cations, **(B)** NO_2^-, the evolution of NO_2^- concentration distribution of three kinds of nitrite solutions: **(C)** $NaNO_2$, **(D)** $Ca(NO_2)_2$, **(E)** $LiNO_2$. The red circle represents the depth of ion aggregation and the yellow circle represents the final depth of ion penetration.

$Ca(NO_2)_2$ solution is slightly larger than that of $NaNO_2$, which explains why $Ca(NO_2)_2$ solution transports faster than $NaNO_2$ solution.

The adsorption of ions on the pore surface can slow down the transport of NO_2^- ions. Therefore, the differences in the adsorption behavior of NO_2^- ions on the pore surface in three kinds of nitrite solutions have been studied and analyzed. The RDFs of the Ca_{sur}-NO_2^- (Ca_{sur} represents the Ca of the channel surface) display the peaks at around 2.45 Å, as shown in Figure 6. When NO_2^- ions pass through the pore surface, Ca_{sur} (Ca on the surface of the pore) will capture the NO_2^- ions and form a stable ion pair with them, reducing the transport speed of NO_2^- ions obviously. By comparing the peak heights, it is found that the Ca_{sur} in $LiNO_2$ solution has the most potent ability to capture NO_2^-, which could slow down the transport speed of NO_2^- most. By comparing the peak heights, it is found that Ca_{sur} in $LiNO_2$

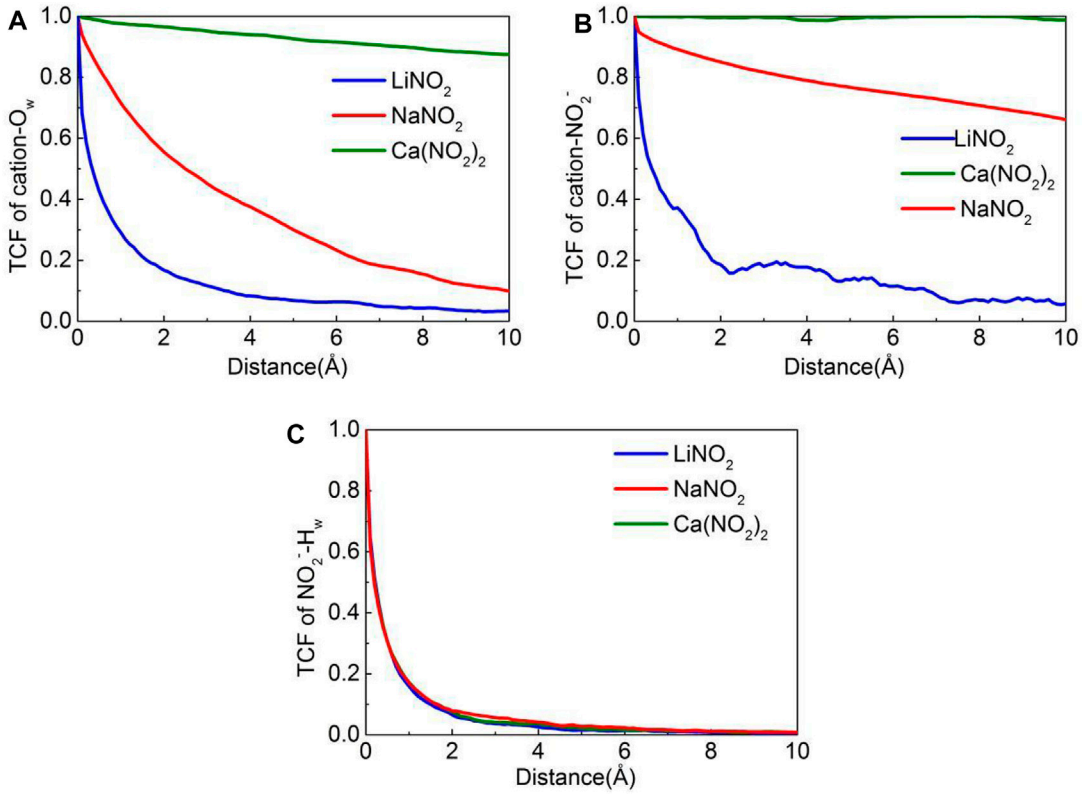

FIGURE 10
Time correlated function (TCF) of **(A)** NO_2^--H_w, **(B)** Casur-NO_2^-, **(C)** Cation-O_w.

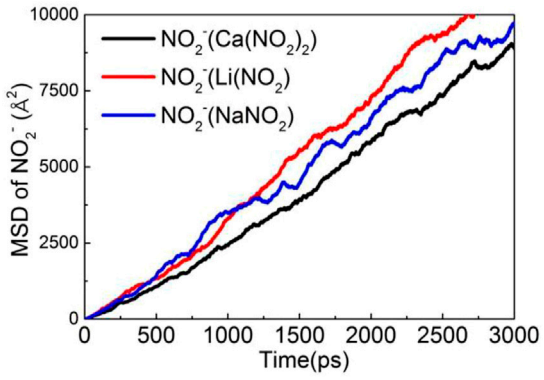

FIGURE 11
MSD of NO_2^- in three kinds of nitrite solution.

solution has the most potent ability to capture NO_2^-, so $LiNO_2$ solution should possess the slowest transport speed. However, the average coordinate number between NO_2^- and Ca_{sur} can be ignored than the other coordinate numbers for all systems. Therefore, the adsorption of ions on the pore channel surface hardly has any significant effect on the transport speed of NO_2^-.

In addition to considering the adsorption of NO_2^- on pore channels surface, the ions pair of nitrite solution in the pore surface should also be considered. In order to trace the local structure of cations in the pore, the RDFs of cation-NO_2^- and cation-O_w have been obtained and shown in Figures 7A,B. The RDFs of cation-O_w and cation- NO_2^- display the prominent peaks, revealing that the cations will form NO_2^--cation-water clusters in nitrite solution. Taking $Ca(NO_2)_2$ solution as an example, the formed clusters will affect the transport speed of nitrite solution shown in Figure 7C. Similarly, the transport behavior of sodium chloride solution in the pores of CSH gel also found the same phenomenon: the formation of clusters of cations and chloride ions in the pores will inhibit the transport behavior of the solution (Zhang et al., 2017).

The Li-O_w (oxygen in water) peak location is much far from the others, and its peak is much lower than the others, shown in Figure 7A, indicating the chemical bond between Li and water is the weakest. Similarly, the chemical bond between Li and NO_2^- is weaker than other bonds, as shown in Figure 7B, indicating that Li has the weakest binding ability with water molecules and NO_2^-. As a result, Li ions cannot form stable clusters to reduce

TABLE 1 The average coordination number (CN).

	NO_2^--H_w	Casur-NO_2^-	Cation-NO_2^-	Cation-O_w
$Ca(NO_2)_2$	4.38	0.04	2.28	5.6
$NaNO_2$	4.27	0.14	1.807	3.9
$LiNO_2$	5.26	0.28	0.48	0

the transport speed compared with Ca and Na ions, which explains why NO_2^- in $LiNO_2$ solution has the fastest transport speed.

In addition to the ionic bonding in the above solution, CSH substrate also affects the transport of rust inhibitor molecules in its nanochannel. Figure 8A shows RDFs of CSH substrate oxygen atom (Os) and CSH cation in inhibitor, the RDFs of cation-O_s display the prominent peaks, revealing that the cations will form O_s-cation clusters in the interface of CSH substrate. Both Na ions and Ca ions have peak values at 2.35 Å, while the peak values of Li ions are far away, indicating that Li ions are not easily adsorbed by CSH substrate. As shown in Figures 8B–D, both Ca and Na ions produce ionic bonding with O_s atoms in the CSH substrate, and NO_2^- and water molecules are also attracted by cations to form O_s-cation-water (NO_2^-) clusters, thus affecting the transport of NO_2^-.

3.3 Dynamics behavior of ions

In order to further analyze the transport behavior of different nitrite solutions in the CSH channel, the number of NO_2^- entering the CSH channel and the evolution of NO_2^- concentration distribution in three nitrite solutions has been calculated, as shown in Figure 9. As shown in Figures 9A,B, the number of cations and NO_2^- in the three nitrite solutions continuously enters the CSH channel with the transmission of the solution, and the ions in $LiNO_2$ has the largest transmission number, followed by $NaNO_2$ and $Ca(NO_2)_2$. Figures 9C–E show the transport of NO_2^- in the channel over time to understand the phenomenon, the red circle represents the depth of ion aggregation, and the yellow circle represents the final depth of ion penetration. The penetration depth of $NaNO_2$ is less than that of the other two nitrite solutions, and NO_2^- ions in $NaNO_2$ are concentrated in about half of the maximum penetration depth, as shown in Figure 9C, which indicates that only a few NO_2^- ions in $NaNO_2$ can arrive at the top of the concave liquid surface. Compared with $NaNO_2$, $Ca(NO_2)_2$ and $LiNO_2$ have the same higher penetration depth. The main difference between them is that NO_2^- in $Ca(NO_2)_2$ solution is mainly distributed in the lower part of the channel, and NO_2^- in $LiNO_2$ solution is mainly distributed in the upper boundary of the channel, as shown in Figures 9D,E. As a result, even the $Ca(NO_2)_2$ and the $LiNO_2$ solution possess the same penetration depths, a greater amount of NO_2^- in $LiNO_2$ solution can be transported more depth. It indicates that $LiNO_2$ can penetrate the microporous channel of cement and reach the surface of reinforcing steel faster to play a promotional role in anti-corrosion.

Atomic dynamics behavior is crucial for the transport behavior of the solution. Simultaneously, the time correlation function is a powerful tool to determine the stability of chemical bonds. Therefore, based on atomic dynamics, the time correlation function (TCF) has been used to evaluate the stability of chemical bonds between ion pairs (Hou et al., 2014). The results are calculated by Eq. 1 and shown in Figure 10. Then the mean square displacement (MSD) is used to visually characterize the diffusion of ions in the pores (Hou and Li, 2014).Where $\delta b\ (t)$ = b(t)-, b(t) is a binary indicator with a value of one if a chemical bond is formed, otherwise a value of 0 instead, at the same time, the faster the TCF curve decays with time, the weaker the bond connection. The decay orders of the cation-O_w TCF and cation -NO_2^- TCF curves presented the same regular, which are $LiNO_2$> $NaNO_2$> $Ca(NO_2)_2$, indicating that the chemical bonds of Li-O_w and Li-NO_2^- are the most vulnerable, respectively, as shown in Figures 10A,B. Therefore, the effect of ion clusters in $LiNO_2$ solution on the transport process is the weakest, and the transport speed of NO_2^- in $LiNO_2$ solution is faster than that in the other two solutions. In addition, the difference of TCF curves of NO_2^--H_w in three nitrite solutions is almost invisible, which indicates that the stability of NO_2^--H_w bond in different nitrite solutions is almost the same, as shown in Figure 10C.

MSD is a measure of ion diffusion velocity, and its slope is directly proportional to the diffusion coefficient. The MSD of the NO_2^- in the three kinds of nitrite solution has been calculated and exhibited in Figure 11. It is clearly shown that the MSD of NO_2^- in the $LiNO_2$ solution is much higher than that of the other two due to the chemical bond between Li-O_w and NO_2^- is the weakest, so it cannot effectively limit its diffusion. Therefore, MSD results once again demonstrate that NO_2^- in $LiNO_2$ solution has the highest diffusion coefficient and the fastest transport speed in the CSH channel during the three kinds of nitrite solution.

4 Conclusion

The transport behavior of three kinds of nitrite corrosion inhibitors in cement microporous channels is investigated based

on MD simulation, and the differences in transport speed have been demonstrated by the local structure and dynamics behavior. The main conclusions are summarized as follows:

1) The transport process and dynamic analysis indicates that the NO_2^- penetration depth of $LiNO_2$ is similar to that of $Ca(NO_2)_2$ but much greater than that of $NaNO_2$. In addition, the NO_2^- in $LiNO_2$ solution is mainly distributed in the upper boundary of the channel, while the NO_2^- in $Ca(NO_2)_2$ solution is mainly distributed in the lower part of the channel. Transport simulations indicate that $LiNO_2$ can penetrate the microporous channel of cement and reach the surface of reinforcing steel faster.
2) An analysis of the local structure of ions in the pore channel reveals that the NO_2^--cation-water and O_s-cation-NO_2^- clusters inhibits solution transport speed. Local structure analysis reveals that Li has the weakest ability to bind water molecules, NO_2^- and CSH substrate, resulting in Li^+ ions cannot form stable clusters to reduce the ion transport speed as Ca and Na ions. In addition, the abortion effect of the channel is negligible because of the minimal coordination number of Ca_{sur}-NO_2^-. Therefore, NO_2^- in $LiNO_2$ solution has the fastest transport speed (Plimpton et al., 2007; Wang et al., 2020c).

Data availability statement

The datasets presented in this study can be found in online repositories. The names of the repository/repositories and accession numbers can be found in the article/Supplementary Material.

Author contributions

XH: Methodology, conceptualization, investigation, Data curation, Writing—original draft. HZ: Writing—review, editing, supervision. RT: Investigation, editing. PW: Methodology, supervision.

Funding

Financial support from National Natural science foundation of China under Grant Nos. U1806225, 52108224, 51908308, Natural science foundation of Shandong Province under Grant ZR2019PEE004, Taishan Scholar Foundation of Shandong Province under Grant Nos. ts20190942, China Postdoctoral Science Foundation under Grant 2019M652345.

Conflict of interest

The authors declare that the research was conducted in the absence of any commercial or financial relationships that could be construed as a potential conflict of interest.

Publisher's note

All claims expressed in this article are solely those of the authors and do not necessarily represent those of their affiliated organizations, or those of the publisher, the editors and the reviewers. Any product that may be evaluated in this article, or claim that may be made by its manufacturer, is not guaranteed or endorsed by the publisher.

References

Ababneh, A., Benboudjema, F., and Xi, Y. (2013). Chloride penetration in nonsaturated concrete. *J. Mater. Civ. Eng.* 15, 183–191. doi:10.1061/(ASCE)0899-1561(2003)15:2(183)

Aydin, O., and Cizmeciglu, Z. (2015). Performance of organic and inorganic substances as inhibitors for chloride-induced corrosion in concrete. *Materials Testing* 57, 85–90. doi:10.3139/120.110680

Bažant, Z. P. (1979). Physical model for steel corrosion in concrete sea structures—Application. *J. Struct. Div.* 105, 1155–1166. doi:10.1061/jsdeag.0005169

Care, S., Nguyen, Q. T., L'Hostis, V., and Berthaud, Y. (2008). Mechanical properties of the rust layer induced by impressed current method in reinforced mortar. *Cem. Concr. Res.* 38, 1079–1091. doi:10.1016/j.cemconres.2008.03.016

Chen, B., Qiao, G., Hou, D., Wang, M., and Li, Z. (2020). Cement-based material modified by *in-situ* polymerization: From experiments to molecular dynamics investigation. *Composites Part B: Engineering* 194, 108036. doi:10.1016/j.compositesb.2020.108036

Cygan, R. T., Liang, J.-J., and Kalinichev, A. G. (2004). Molecular models of hydroxide, oxyhydroxide, and clay phases and the development of a general force field. *J. Phys. Chem. B* 108, 1255–1266. doi:10.1021/jp0363287

Devi, M., and Kannan, K. (2013). Evaluation of corrosion inhibition performance of zinc oxide and sodium nitrite in quarry dust concrete. *Asian J. Chem.* 25, 8690–8696. doi:10.14233/ajchem.2013.15237

Diamanti, M. V., del Curto, B., Ormellese, M., Bolzoni, F., and Cilluffo, G. (2017). *On the use of nitrates as corrosion inhibitors for concrete rebars*. Italy: Metallurgia Italiana, 55–58.

Dauber-Osguthorpe, P., Roberts, V. A., Osguthorpe, D. J., Wolff, J., Genest, M., and Hagler, A. T. (1988). Structure and energetics of ligand binding to proteins: *Escherichia coli* dihydrofolate reductase-trimethoprim, a drug-receptor system. *Proteins.* 4, 31–47. doi:10.1002/prot.340040106

Garces, P., Saura, P., Zornoza, E., and Andrade, C. (2011). Influence of pH on the nitrite corrosion inhibition of reinforcing steel in simulated concrete pore solution. *Corros. Sci.* 53, 3991–4000. doi:10.1016/j.corsci.2011.08.002

Garces, P., Saura, P., Mendez, A., Zornoza, E., and Andrade, C. (2008). Effect of nitrite in corrosion of reinforcing steel in neutral and acid solutions simulating the electrolytic environments of micropores of concrete in the propagation period. *Corros. Sci.* 50, 498–509. doi:10.1016/j.corsci.2007.08.016

González, J. A., Ramı´rez, E., and Bautista, A. (1998). Protection of steel embedded in chloride-containing concrete by means of inhibitors. *Cem. Concr. Res.* 28, 577–589. doi:10.1016/s0008-8846(98)00014-3

Hazehara, H., Katpady, D. N., Soeda, M., Okabe, Y., and Era, K. (2020). Neutralization inhibition mechanism of lithium nitrite and its effect on the microstructure of mortar. *Constr. Build. Mater.* 264, 120586. doi:10.1016/j.conbuildmat.2020.120586

Hou, D. S., and Li, Z. J. (2014). Molecular dynamics study of water and ions transport in nano-pore of layered structure: A case study of tobermorite. *Microporous Mesoporous Mater.* 195, 9–20. doi:10.1016/j.micromeso.2014.04.011

Hou, D. S., Ma, H. Y., Yu, Z., and Li, Z. J. (2014). Calcium silicate hydrate from dry to saturated state: Structure, dynamics and mechanical properties. *Acta Mater.* 67, 81–94. doi:10.1016/j.actamat.2013.12.016

Hou, D., Li, T., and Wang, P. (2018). Molecular dynamics study on the structure and dynamics of NaCl solution transport in the nanometer channel of CASH gel. *ACS Sustain. Chem. Eng.* 6, 9498–9509. doi:10.1021/acssuschemeng.8b02126

Hou, D., Jia, Y., Yu, J., Wang, P., and Liu, Q. (2018). Transport properties of sulfate and chloride ions confined between calcium silicate hydrate surfaces: A molecular dynamics study. *J. Phys. Chem. C* 122, 28021–28032. doi:10.1021/acs.jpcc.8b07484

Hori, T., Kitagawa, A., and Nakamura, Y. (1991). The concrete carbonation inhibiting effect of mortar containing lithium nitrite. *Cem. Sci. Concr. Technol.* 45, 550–555.

Krolikowski, A., and Kuziak, J. (2011). Impedance study on calcium nitrite as a penetrating corrosion inhibitor for steel in concrete. *Electrochimica Acta* 56, 7845–7853.

Li, J. H., Zhao, B., Hu, J., Zhang, H., Dong, S. G., Du, R. G., and Lin, C. J. (2015). Corrosion inhibition effect of D-sodium gluconate on reinforcing steel in chloride-contaminated simulated concrete pore solution. *Int. J. Electrochem. Sci.* 10, 956–968.

Li, D., Zhao, W., Hou, D., and Zhao, T. (2017). Molecular dynamics study on the chemical bound, physical adsorbed and ultra-confined water molecules in the nano-pore of calcium silicate hydrate. *Constr. Build. Mater.* 151, 563–574. doi:10.1016/j.conbuildmat.2017.06.053

Mandal, S., Singh, J. K., Lee, D. E., and Park, T. (2020). Effect of phosphate-based inhibitor on corrosion kinetics and mechanism for formation of passive film onto the steel rebar in chloride-containing pore solution. *Materials* 13, 3642. doi:10.3390/ma13163642

Nonat, A. (2004). The structure and stoichiometry of C-S-H. *Cem. Concr. Res.* 34, 1521–1528. doi:10.1016/j.cemconres.2004.04.035

Nonat, A., and Lecoq, X. (1998). "The structure, stoichiometry and properties of C-S-H prepared by C3S hydration under controlled condition," in *Nuclear magnetic resonance spectroscopy of cement-based materials*. Editors P. Colombet, H. Zanni, A.-R. Grimmer, and P. Sozzani (Berlin, Heidelberg: Springer), 197–207.

Okeniyi, J. O., Omotosho, O. A., Ajayi, O. O., and Loto, C. A. (2014). Effect of potassium-chromate and sodium-nitrite on concrete steel-rebar degradation in sulphate and saline media. *Constr. Build. Mater.* 50, 448–456. doi:10.1016/j.conbuildmat.2013.09.063

Ormellese, M., Bolzoni, F., Goidanich, S., Pedeferri, M. P., and Brenna, A. (2011). Corrosion inhibitors in reinforced concrete structures Part 3-migration of inhibitors into concrete. *Corrosion Engineering Science and Technology* 46, 334–339. doi:10.1179/174327809x419230

Page, C. L., and Treadaway, K. W. J. (1982). Aspects of the electrochemistry of steel in concrete. *Nature* 297, 109–115. doi:10.1038/297109a0

Page, C. L. (1975). Mechanism of corrosion protection in reinforced concrete marine structures. *Nature* 258, 514–515. doi:10.1038/258514a0

Plimpton, S., Crozier, P., and Thompson, A. (2004). *LAMMPS-large-scale atomic/molecular massively parallel simulator*. Sandia National Laboratories, 43.

Qian, S., and Cusson, D. (2004). Electrochemical evaluation of the performance of corrosion-inhibiting systems in concrete bridges. *Cem. Concr. Compos.* 26, 217–233. doi:10.1016/s0958-9465(03)00041-6

Reou, J. S., and Ann, K. Y. (2008). The electrochemical assessment of corrosion inhibition effect of calcium nitrite in blended concretes. *Mater. Chem. Phys.* 109, 526–533. doi:10.1016/j.matchemphys.2007.12.030

Ryu, H. S., Singh, J. K., Lee, H. S., and Park, W. J. (2017). An electrochemical study to evaluate the effect of calcium nitrite inhibitor to mitigate the corrosion of reinforcement in sodium chloride contaminated Ca(OH)(2) solution. *Advances in Materials Science and Engineering* 2017, 1–14. doi:10.1155/2017/62651846265184

Ryu, H. S., Singh, J. K., Lee, H. S., Ismail, M. A., and Park, W. J. (2017). Effect of LiNO2 inhibitor on corrosion characteristics of steel rebar in saturated Ca(OH)(2) solution containing NaCl: An electrochemical study. *Constr. Build. Mater.* 133, 387–396. doi:10.1016/j.conbuildmat.2016.12.086

Schiessl, P., Mayer, T. F., and Osterminski, K. (2008). Influence of the chromate content in cement on the corrosion behaviour of steel in concrete. *Materials and Corrosion* 59, 115–121. doi:10.1002/maco.200804160

Sun, C. T., Chen, M. S., Zheng, H. B., Zhang, P., Li, Y. T., and Hou, B. R. (2019). The effect of amino-alcohol-based corrosion inhibitors on concrete durability. *Can. J. Civ. Eng.* 46, 771–776. doi:10.1139/cjce-2018-0482

Soylev, T. A., and Richardson, M. G. (2008). Corrosion inhibitors for steel in concrete: State-of-the-art report. *Constr. Build. Mater.* 22, 609–622. doi:10.1016/j.conbuildmat.2006.10.013

Thangavel, K., and Rengaswamy, N. S. (1998). Relationship between chloride/hydroxide ratio and corrosion rate of steel in concrete. *Cem. Concr. Compos.* 20, 283–292. doi:10.1016/s0958-9465(98)00006-7

Wang, P., Qiao, G., Hou, D., Jin, Z., Wang, M., Zhang, J., and Sun, G. (2020b). Functionalization enhancement interfacial bonding strength between graphene sheets and calcium silicate hydrate: Insights from molecular dynamics simulation. *Constr. Build. Mater.* 261, 120500. doi:10.1016/j.conbuildmat.2020.120500

Wang, P., Qiao, G., Guo, Y., Zhang, Y., Hou, D., Jin, Z., Zhang, J., Wang, M., and Hu, X. (2020a). Molecular dynamics simulation of the interfacial bonding properties between graphene oxide and calcium silicate hydrate. *Constr. Build. Mater.* 260, 119927. doi:10.1016/j.conbuildmat.2020.119927

Wang, P., Qiao, G., Zhang, Y., Hou, D., Zhang, J., Wang, M., Wang, X., and Hu, X. (2020c). Molecular dynamics simulation study on interfacial shear strength between calcium-silicate-hydrate and polymer fibers. *Constr. Build. Mater.* 257, 119557. doi:10.1016/j.conbuildmat.2020.119557

Yang, J., Jia, Y., Hou, D., Wang, P., Jin, Z., Shang, H., Li, S., and Zhao, T. (2019). Na and Cl immobilization by size controlled calcium silicate hydrate nanometer pores. *Constr. Build. Mater.* 202, 622–635. doi:10.1016/j.conbuildmat.2019.01.066

Yu, J., Zheng, Q., Hou, D. S., Zhang, J. R., Li, S. C., Jin, Z. Q., Wang, P., Yin, B., and Wang, X. P. (2019). Insights on the capillary transport mechanism in the sustainable cement hydrate impregnated with graphene oxide and epoxy composite. *Composites Part B: Engineering* 173, 106907. doi:10.1016/j.compositesb.2019.106907

Zhang, P., Hou, D. S., Liu, Q., Liu, Z. L., and Yu, J. (2017). Water and chloride ions migration in porous cementitious materials: An experimental and molecular dynamics investigation. *Cem. Concr. Res.* 102, 161–174. doi:10.1016/j.cemconres.2017.09.010